



# Behavior of Geogrid Reinforced and Unreinforced Non-connected Pile Raft Foundation

Mohammad Ghanbar Dezfouli<sup>1</sup> · Masoud Dehghani<sup>1</sup> · Adel Asakereh<sup>1</sup> · Behzad Kalantari<sup>1</sup>

Received: 24 April 2018 / Revised: 1 September 2018 / Accepted: 3 October 2018 / Published online: 16 October 2018  
© Iran University of Science and Technology 2018

## Abstract

Presence of reinforcement elements such as geogrid in the cushion layer of the non-connected pile raft foundation changes the load transition mechanism and the portion of piles and raft from the total load. In this paper, experimental studies have been conducted on a non-connected pile raft foundation located in a sandy soil. The effect of parameters such as piles spacing, the thickness of cushion, position, length and number of geogrid layers on the behavior of load settlement, the portion of piles and raft from the total load, and distribution of axial and frictional stress along the pile and position of neutral axis were studied. The results showed that in unreinforced cases, with an optimum cushion thickness and piles spacing, the lowest settlement is observed. The use of geogrid in the cushion layer increases the bearing capacity and the portion of the piles from the total load and led to a move up in the neutral axis to the top of the piles. The optimum position and length of the first and second geogrid layers have also been studied.

**Keywords** Non-connected pile raft · Geogrid · Experimental study · Sandy soil · Cushion

## 1 Introduction

In recent years, several studies have been conducted on reinforced soil to increase the bearing capacity and reduce settlement using vertical elements such as piles, micro piles, stone columns and horizontal elements such as geosynthetics. Usually, pile foundations are used to back up the superstructures by transferring the load from the soft surface layers to the firmer deep underground layers [1–3]. In special geotechnical conditions or heavy loads, the composition of the pile with the raft is desirable to increase the bearing capacity and reduce settlement. Therefore, the concepts of connected and non-connected pile raft foundation are studied based on the connection of pile to raft. In the pile raft

system (connected and non-connected), both pile and raft contribute to transferring the load to the underlying layers. In non-connected pile raft foundation, the cushion plays a significant role in transferring the load from the upper structure to the raft and the pile. Therefore, geometrical and mechanical properties of this layer have significant effects on the behavior of non-connected pile raft [4]. A number of studies have been conducted on the non-connected pile rafts using numerical models [5–13], analytical methods [14–17] 1 g laboratory tests [18, 19], centrifuge models [20, 21] and large-scale models [22]. Today, the composition of horizontal elements (geogrids) and vertical elements (pile) has been widely used, which may refer to the foundation located on sand columns and geogrid [23], or structures located on piles and geogrids [24–27].

Fioravante et al. [28] studied the effect of stiffness of the pile and soil and the cushion on the behavior of non-connected pile raft using centrifuge modeling. The results showed that the presence of cushion caused a negative friction in the upper part of the pile and will create a positive friction in the lower part. The results also proved that the transfer of the load is carried out by the cushion. When the stiffness of the cushion is reduced, the efficiency of the pile raft decreases.

✉ Adel Asakereh  
asakereh@hormozgan.ac.ir

Mohammad Ghanbar Dezfouli  
m.ghanbardezfooli.phd@hormozgan.ac.ir

Masoud Dehghani  
m.dehghani@hormozgan.ac.ir

Behzad Kalantari  
kalantari@hormozgan.ac.ir

<sup>1</sup> Department of Civil Engineering, Hormozgan University, Bandar Abbas, Iran

Tradigo et al. [7] studied a 3D finite element model of connected and non-connected pile raft and compared them. Effects of some parameters such as the thickness of cushion and number of piles on the behavior of the system and distribution of axial stress in pile length were investigated. The results showed that in non-connected pile raft, negative frictional stresses are created at the upper part of the piles. Further, the neutral axis has moved downward by increasing the cushion thickness.

Deb et al. [23] explored analytical relations to determine the behavior of foundation located on geogrid layers and stone columns. A spring model was utilized to simulate elements of stone columns. The soil behavior under geogrids is shown in the Kelvin–Voight model. The results showed that the use of geogrid layers in the space between the sandy columns and the raft is effective in reducing settlement. The first layer of geogrid also played a more important role in reducing settlement. The use of geogrid layers resulted in reducing the transmission of stress to the soft soil around the stone column.

King et al. [22] studied the large-scale behavior of pile raft with geogrid. They conducted their studies on two reservoirs (one with geogrid and the other without it). The findings showed that lateral displacement of soil at the front of piles (external medium) was less than the lateral displacement of soil between piles, and small bending stresses might occur in piles in the test without geogrid. Under lower loads, the rate of applied forces is close to each other when using geogrid and without it, while following the rise of applied loads, the applied force to piles in testing with geogrid is increased faster than experiment without geogrid. The axial force of piles varies nonlinearly along the pile. The negative friction force is formed at the upper part of the piles and this force is less in tests with geogrid compared with the tests without geogrid. Also under the ultimate load, the earth pressures on the central cap were greater in the test with geogrid, while its subsoil carried less earth stress as compared with those for the test without geogrid. Moreover, the maximum earth pressure was obviously distributed along the edge of central cap in the test with geogrid.

Saeedi Azizkandi et al. [29] conducted some centrifuge tests on a group of installed piles and found that the relative density ratio of soil has an important role in determining the pile–soil–pile interaction. The reason for decrease of pile–soil–pile interaction in a small value of relative density can be explained as the occurrence of relative displacement between the interface of soil and pile which in turn causes a decrease in the pile–soil interaction and consequently decreases the pile–soil–pile interaction.

In seismically active areas, due to the rigidity of the intersection, devastating stresses will be cumulated at the pile cap which can lead to a structural failure at the junction of pile and raft. Also, in most design codes (ASTM 1969, British

Standard 1986, Singapore Code2002), strong limitations have been imposed for the allowable stresses in the piles which may lead to uneconomical design of the foundation system [21].

A number of researchers studied the dynamic response of the connected and non-connected pile raft foundation system under seismic loads. The result indicate that the internal forces, including axial forces and the bending moment, along the piles were small in the non-connected pile raft foundation compared to the connected pile raft foundation and the effects of superstructure frequencies on these internal forces were minimal [30]. In connected piled raft, piles bear higher moments and lateral loads and reduce lateral movements more effectively. Superstructure tends to increase the pile moment and raft inclination where the frequency effect is also critically important [31].

In this study, the presence of layers of geogrid in cushion was investigated. The presence of geogrid in cushion changes the behavior of pile raft system. There is little research about the use of geogrid layers in the cushion, which requires a comprehensive review. In the present paper, a laboratory investigation on the pile raft foundation with reinforced cushion by a geogrid layer is conducted. So, the behavior of the non-connected pile raft in the reinforced and unreinforced cases will be discussed by changing the parameters of the thickness of the cushion and the piles spacing. In addition, the optimum location of the first and second layers of the geogrid in the cushion and the optimum length of these layers have been investigated.

## 2 Experimental Setup

All tests were conducted using the instrumentation shown in Figs. 1 and 2. Figure 1 shows a schematic illustration of the boundary conditions, the location of piles and LDVT sensors

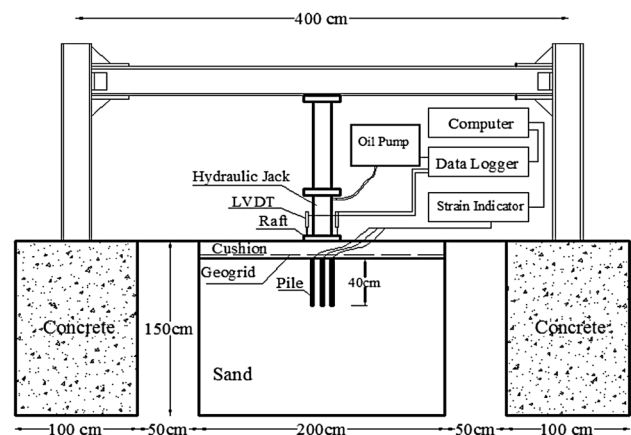


Fig. 1 Cross-section of test model

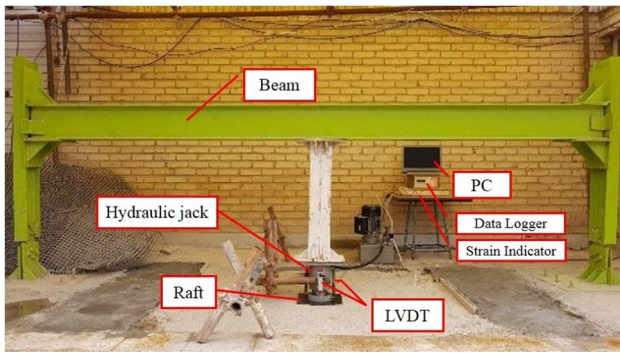


Fig. 2 General view of the testing apparatus with its attachments

in the test trench. Figure 2 shows a photo of the hydraulic jack, loading frame, data logger, and strain indicator that are described below:

### 2.1 Loading System

The loading system includes a hydraulic jack, loading frame and control unit. The load is applied by an automatic hydraulic jack with a capacity of 15 tons and a course of 15 cm with a controlled rate. The hydraulic jack is equipped with a pressure sensor that transmits the data related to pressure and force to the data logger. The loading frame consists of two columns of IPE200 connected to concrete weights of 7.5 tons buried in soil and a horizontal beam of 4 m in length from 2IPE240. A borehole with a length of 2 m, a width of 2 m and depth of 1.5 m was drilled to conduct tests on the ground.

### 2.2 Recording Data and Instrumentation

To record the displacements, two LVDTs with a precision of 0.001 mm are used. The readings of forces and displacements are transmitted to a data logger and recorded at a rate of one reading per second on the PC. To ensure the results and performance of the loading equipment, before each test, all equipment are calibrated. So, a load cell is used to calibrate the pressure gauge of the jack and a micrometer is used for LVDT calibration. To record the stresses of the piles during loading, in the direction of the axis of the central pile (P1) and the corners (P3), strain gauges were installed at intervals of 10 cm. In addition, at the top of the lateral pile (P2), a strain gauge is also installed. Three strain gauges were placed in the pile environment at each level at 120 degrees from the center of the pile. The arrangement of strain gauges is shown in Fig. 3. The reading information of strain gauge is transmitted to a strain indicator and one reading is recorded every second.

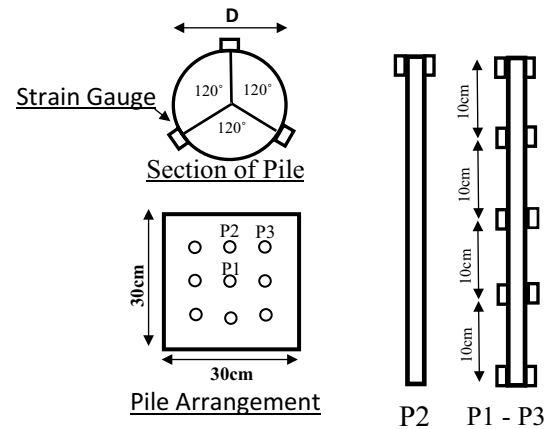


Fig. 3 Arrangement and location of piles and strain gauge

## 3 Material

### 3.1 Sand

Two types of silicate sand have been used as sandy bed and cushion. The properties of sands are shown in Table 1. The particle size distributions are shown in Fig. 4. According to the unified soil classification system (USCS), both types of soils are classified as poorly graded sand (SP).

### 3.2 Pile and Raft

To model the raft, a square metal plate with the width of 300 mm and the thickness of 25 mm has been used. To model the piles, an aluminum tube with an external diameter of 22 mm and thickness of 1 mm with an elastic modulus of 70 GPa has been used. Bolton et al. [32] and Gui et al. [33, 34] investigated the effect of particle size on the behavior of pile raft and concluded that if the ratio of the pile diameter to the  $D_{50}$  of the soil is more than 20 times, the particle size has an ignorable effect on the results. In the present study, this ratio is equal to 37, which is suitable for comparing the results of this study with other studies on the pile raft.

Table 1 Properties of soils

Parameter	Unit	Bed soil	Cushion
Specific gravity	–	2.66	2.61
Maximum dry unit weight	kN/m <sup>3</sup>	17.7	16.52
Minimum dry unit weight	kN/m <sup>3</sup>	13.38	13.62
$D_{50}$	mm	0.6	2.1
Cc	–	0.5	1.14
Cu	–	2.33	2.94

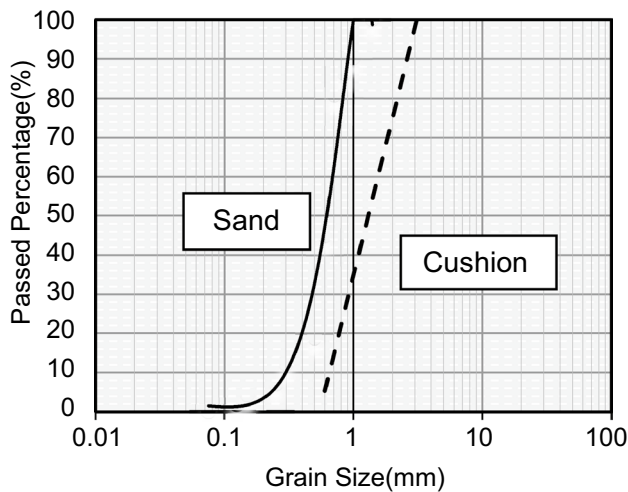


Fig. 4 Particle size distribution

### 3.3 Geogrid

In all series of tests, bi-directional geogrids are used. The properties of geogrid used in this study are shown in Table 2.

## 4 Tests' Preparation

To obtain a uniform soil bed, the method of raining in the air and slapping by the tamper in 10 cm layers was used. In this method, first, the amount of soil required for each layer is weighed and uniformly poured into the test trench and then compacted by the tamper to reach the desired density. To control the uniformity of unit weight in the depth of the soil bed, cube boxes are placed at different depths of the soil bed and the unit weights are measured. After each test, the entire soil is depleted and prepared for the next test by the manner described above. This method makes the tests accurate and repeatable if necessary.

After preparing the soil bed, the piles are slowly inserted into the soil by the jack. The penetration rate of the piles in the soil must be as slow as possible to prevent disturbance of the soil. To place the piles in the proper place, a metal shingle with holes adapted to the location of the piles is used. This metal plate is placed on the sand and the piles

Table 2 Index properties of geogrid

Parameter	Unit	Value
Thickness	mm	1.8
Mass per unit area	Kg/m <sup>2</sup>	0.532
Ultimate tensile strength	kN/m	7.6
Aperture size	mm	23

are placed in the position of the holes in the soil. After the placement of all the piles, the shingle is removed.

In tests with geogrid, after preparing the sand bed where the piles are placed, the geogrid layer is placed on the sand surface and then the cushion layer is poured and tamped on the geogrid like the sandy bed. The relative density of the sandy bed and the cushion is 60% and 90%, respectively.

After preparing the soil sample, the raft is placed on it and the cylinder of the jack is placed in the center of the plate to prevent the load application with eccentricity. Two LVDTs are used to measure the deformation during loading. In each test, loading is gradually applied to the soil in steps of 200 kg. This load is kept constant on the jack until the settlement changes become negligible. During loading and every second, the measure of load, settlement and strain of the piles are recorded.

## 5 Test Procedures

A schematic view of the tests is shown in Fig. 5. In addition, a summary of reinforced and unreinforced tests is shown in Table 3.

Twenty-four tests were conducted in reinforced and unreinforced conditions and a series of repeated tests were performed to ensure the accuracy of the tests. In total, 33 tests were carried out in this study.

All variables used in this study are expressed in non-dimensional form. These parameters are  $H/B$ ,  $S/D$ ,  $U/H$ ,  $h/H$  and  $L/B$ .  $B$  is the footing width,  $H$  is the thickness of cushion,  $S$  is piles spacing,  $D$  is the diameter of piles,  $U$  is the distance between the first layer of geogrid from sand bed,  $h$  is the distance between the second layer of the geogrid from sand bed and  $L$  is the length of geogrid.

Tests are carried out in four series. In series 1, the aim is to study the effect of cushion height ( $H/B$ ) and pile spacing ( $S/D$ ) to obtain optimum values of  $H/B$  and  $S/D$  in unreinforced cases. Different thicknesses of the cushion

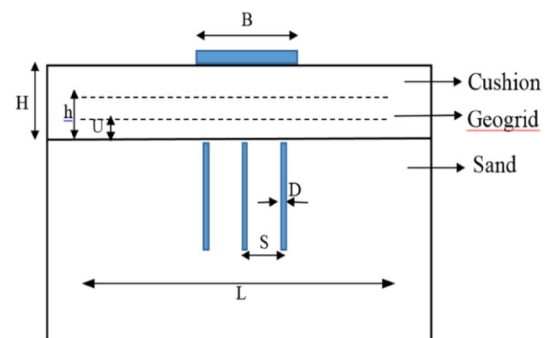


Fig. 5 Geometry of the tests

**Table 3** Test program

Test series	<i>H/B</i>	<i>S/D</i>	<i>U/H</i>	<i>h/H</i>	<i>L/B</i>	No. of geogrids	No. of tests
1	0.17–0.34–0.5	2–4–6	–	–	–	0	12
2	0.34	4	0–0.3–0.6–0.9	–	6	1	4
3	0.34	4	0	0.3–0.6–0.9	6	2	3
4	0.34	4	0	0.6	5–4–3–2–1	2	5

(*H/B* = 0.17, 0.34, 0.5) and different piles spacing (*S/D* = 2, 4, 6) were studied in these cases.

In the series 2, using the optimum values of *S/D* and *H/B* obtained from series 1, the optimum location of the first layer of geogrid in cushion was determined. The first layer of the geogrid was placed in positions of *U/H* = 0, 0.3, 0.6, 0.9. The length of the layer of the geogrid in this case was equal to *L* = 6*B*. In series 3, using the optimum values obtained from the first and second series of the tests, the optimum location of the second layer of geogrid in the cushion was determined. For this purpose, the second layer of the geogrid was placed at positions of *h/H* = 0.3, 0.6, 0.9. Finally, in series 4, the optimum length of geogrid was determined. In this series of tests, the various lengths of layers of geogrid were considered as (6–5–4–3–2–1) \* *B*.

## 6 Results and Discussions

The results of the tests are presented in two reinforced and unreinforced cases. Bearing pressure versus normalized settlement, the portion of piles from the total load and distribution of axial stress in the pile length will be discussed. In unreinforced case, the optimum thickness of the cushion and the optimum piles spacing and in the reinforced case, the optimum position of the first layer of the geogrid, the optimum position of the second layer of the geogrid and the optimum length of geogrids were obtained.

### 6.1 Unreinforced Cases

#### 6.1.1 Effect of Cushion Thickness

Figure 6 shows the variations of bearing pressure versus normalized settlement in cases of *H/B* = 0.17, 0.34 and 0.5. As it is seen in *S/D* = 2, 4, 6, with increasing the *H/B*, bearing pressure is increased. Due to the distribution of load, with increasing the thickness of the cushion, the high stress in the cushion (material with higher density) and lower stress in the lower sandy bed (material with a lower density) are formed, which plays an effective role in increasing the bearing pressure.

To better understand the effect of cushion thickness, the variation of bearing pressure versus *H/B* in normalized

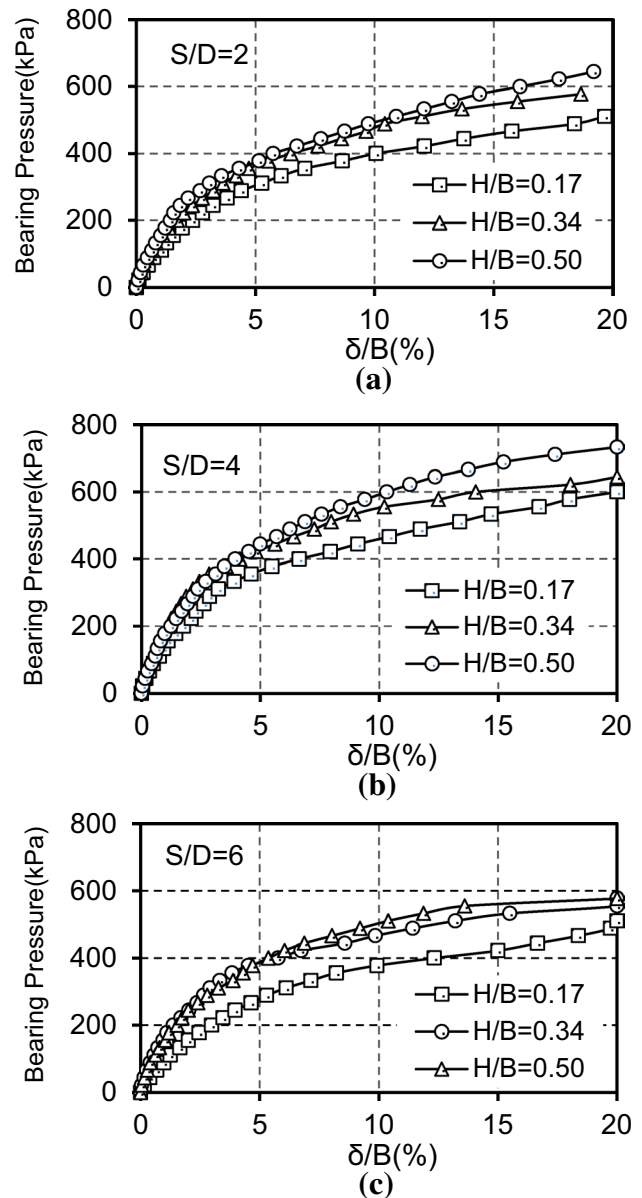


**Fig. 6** Variation of bearing pressure versus normalized settlement for different thicknesses of the cushion at **a** *S/D* = 2, **b** *S/D* = 4, **c** *S/D* = 6

settlement of 2%, 5% and 10% is shown in Fig. 7. As can be seen, with increasing the *H/B*, the slope of first and second part of the curve is not the same. The factor that creates

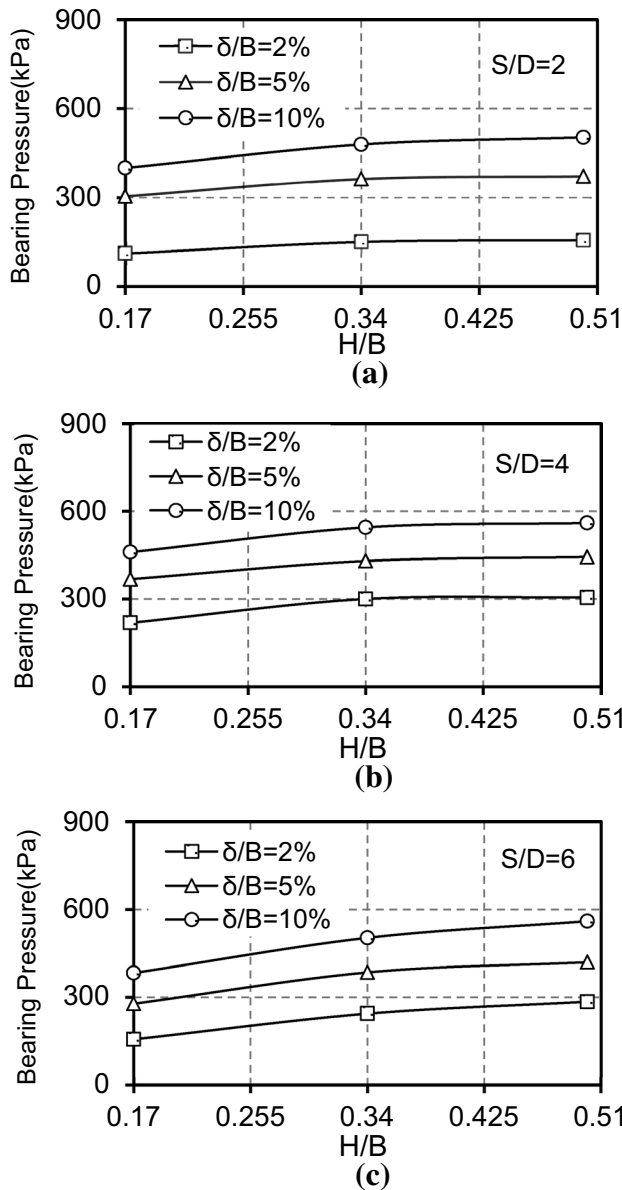


**Fig. 7** Variation of the bearing pressure versus  $H/B$  in normalized settlements (2%, 5% and 10%) at **a**  $S/D=2$ , **b**  $S/D=4$ , **c**  $S/D=6$

this behavior is the arching effect. This effect is imperfectly formed in a specific thickness of the cushion.

Jenck et al. [35] suggested that a full arching occurs only when the  $H/S$  ( $H$ =height of cushion and  $S$ =spacing between piles) is greater than 1.6. Also, BS 8006 [36] suggested that lowest thickness of the cushion for forming partial and full soil arching is 0.7 and 1.4, respectively. Accordingly, for  $S/D=2$  and 4, a partial arching in  $H/B=0.17$  and a full arching in  $H/B=0.34$  and 0.5 are observed. As can be seen in Fig. 7a, b, the slope of the first portion of the curve (with increase of  $H/B$  from 0.17 to 0.34) is more than the first portion of the curve (with increase of  $H/B$  from 0.34 to 0.5). This phenomenon in high settlements (normalized

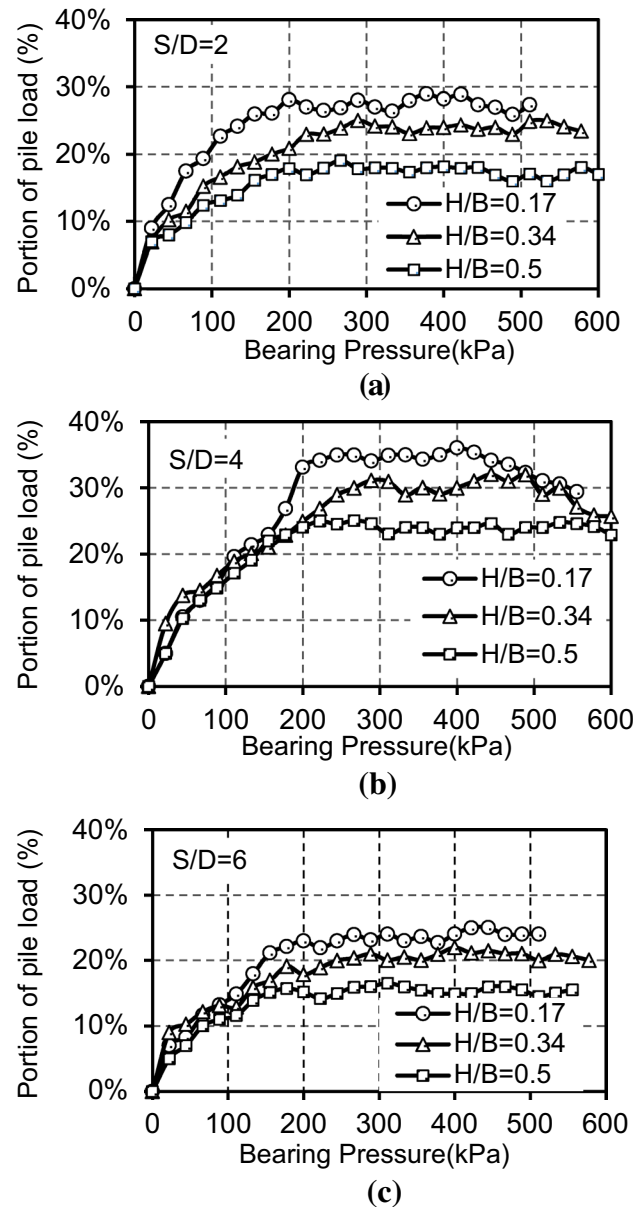


**Fig. 8** Share of the piles from total load for different thicknesses of the cushion: **a**  $S/D=2$ , **b**  $S/D=4$ , **c**  $S/D=6$

settlement between 5 and 10%) is more visible as full arching does not occur because of low load and settlement. In  $S/D=6$  and  $H/B=0.50$ , a full arching occurs. So it can be seen in Fig. 7c that there are no obvious differences between the slopes of first and second portions of curves.

Figure 8 shows the portion of the piles from the total load during loading. The axial forces in piles were calculated based on the measured axial strain in the piles by the strain gauge at the tip of them. The axial force can be calculated by  $N = \epsilon_p E_p A_p$  where  $\epsilon_p$  is the axial strain in pile,  $E_p$  is the elastic modulus of the pile and  $A_p$  is the net cross-section of piles. As it can be seen, in all causes ( $S/D=2, 4, 6$ ), the

increase in cushion thickness results in reducing the portion of piles from the total load. In the early stages of loading, the portion of the piles is small. With the increase in the load, the portion of piles increase rapidly and remains at a constant value. By increasing the thickness of the cushion, more of the load on the cushion is depleted, which causes less force to apply on the pile.

The maximum portion of piles, in  $S/D=4$  and  $H/B=0.17$ , equals to 34% and the minimum, in  $S/D=6$  and  $H/B=0.5$ , equals to 14%. At low stress levels, change in the thickness of the cushion has an insignificant effect on the portion of piles. This effect is more evident at a high stress level.

Figures 9 and 10 show the effect of the thickness of the cushion on the axial and frictional stress distribution in the central pile (P1) and corner piles (P3) at a medium load of 311 kPa in  $S/D=4$ . The reason for the choice of  $S/D=4$  is that at this distance minimum settlement and the maximum bearing pressure are observed.

Because part of the load tolerated by the soil around the piles is transmitted to the piles, the maximum stress applied to the piles does not occur at the tip of the piles,

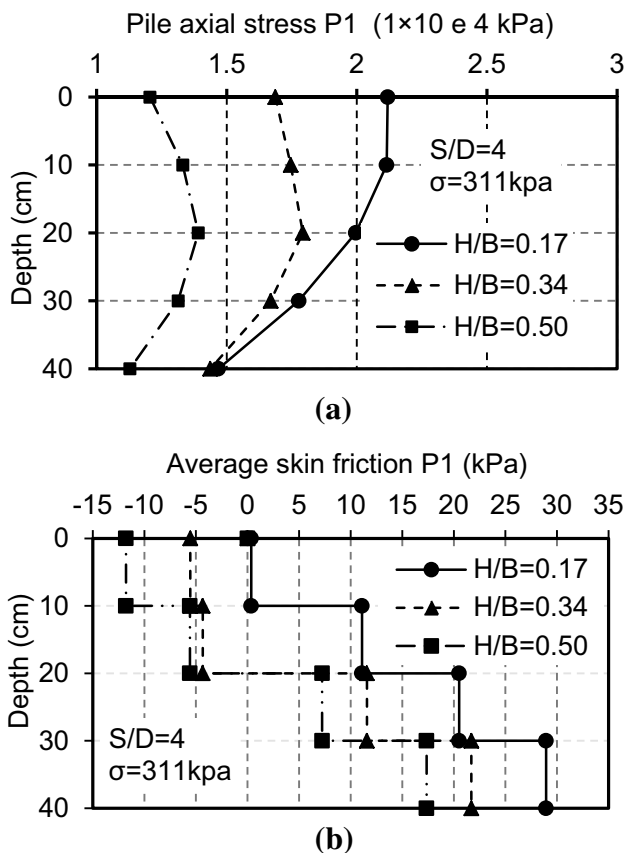


Fig. 9 Variations of axial stress and frictional stress along the central pile (P1) in different thicknesses of the cushion ( $S/D=4$  and  $\sigma=311$  kPa). a Distribution of the axial stress along the pile. b Distribution of the frictional stress along the pile

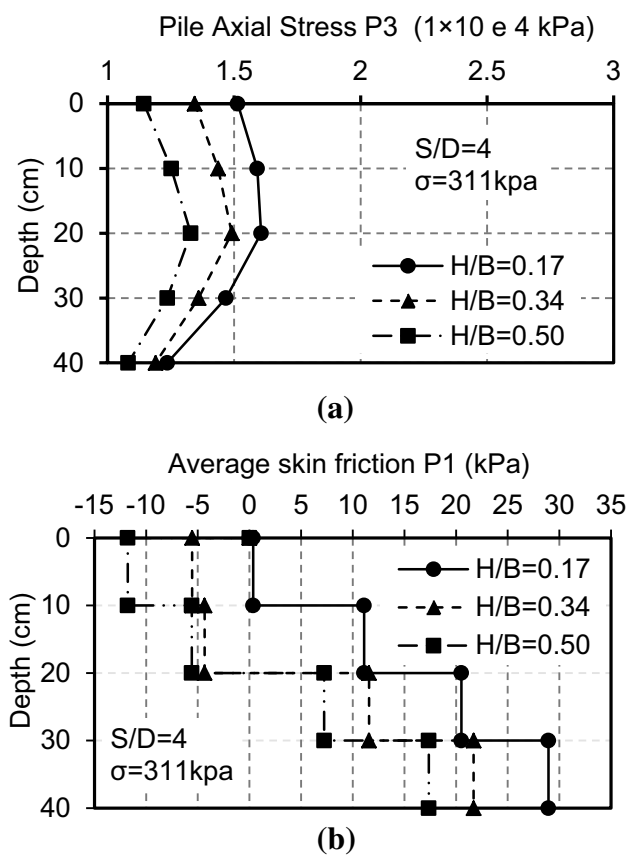


Fig. 10 Variations of axial stress and frictional stress along the corner piles (P3) in different thicknesses of the cushion ( $S/D=4$  and  $\sigma=311$  kPa). a Distribution of the axial stress along the pile. b Distribution of the frictional stress along the pile

and a negative friction occurs at the upper part of the piles. In the upper part of the piles, the displacement of the soil is more than the displacement of the pile that results in the formation of a negative friction and formation of a positive friction in the bottom of the pile. Negative skin friction at the upper part of the piles is much less than the positive skin friction at the lower part of piles. A place in the pile where the displacement of the soil and pile is the same as the location of the transfer of negative friction to the positive friction is called neutral axis. In this axis, the greatest axial force is created in the pile. As the thickness of the cushion increases, the amount of frictional stress increases in the upper part of the pile, and the neutral axis is moved downward. As it was shown previously in Fig. 8, the increase of the thickness of the cushion results in reducing the portion of piles from the total load, so less force has been transmitted into the piles and the deformation of the piles is reduced compared with the soil, which increases the negative friction.

As shown in Figs. 9a and 10a, the central pile tolerates more force compared with the corner piles. In addition, in the upper part of the corner piles there is more

negative friction compared with the central pile, so the neutral axis in the corner piles is at a lower level than the central pile.

### 6.1.2 Effect of Pile Spacing

Figure 11 shows the effect of pile spacing on bearing pressure at the normalized settlement 2%, 5% and 10%. As it is seen, increase of  $S/D$  from 2 to 4 leads to increase in bearing pressure and the increase of  $S/D$  from 4 to 6 leads to decrease of bearing pressure. In all cases, the minimum

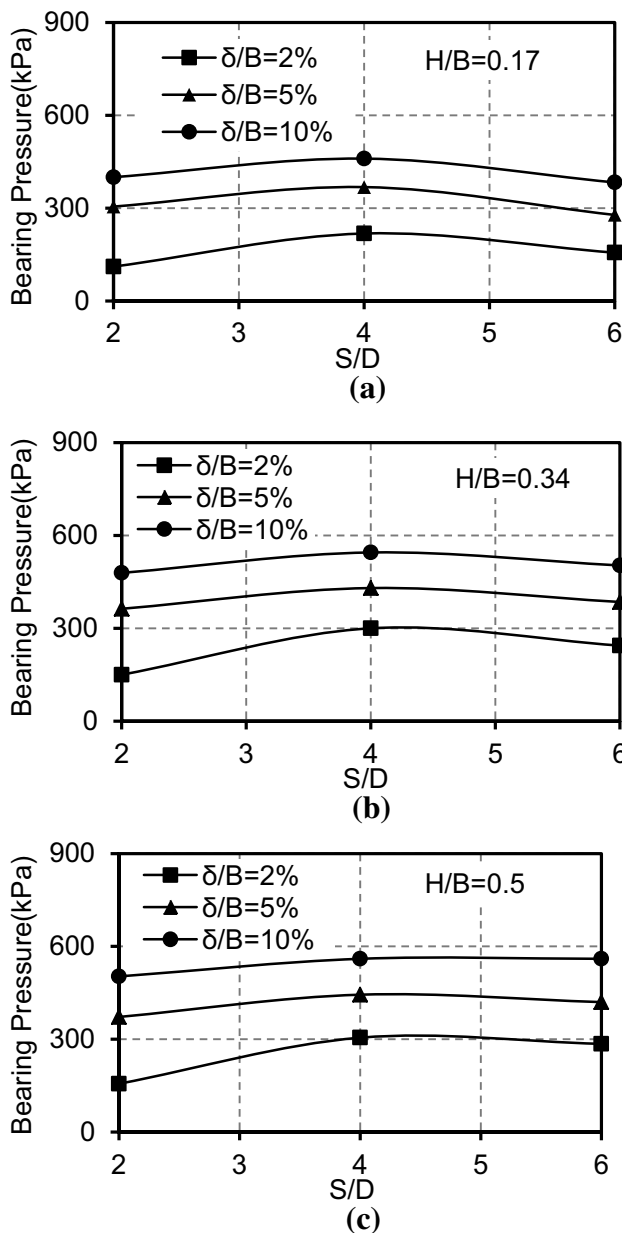


**Fig. 11** Variation of bearing pressure versus  $S/D$  in normalized settlements (2%, 5% and 10%) for **a**  $H/B=0.17$ , **b**  $H/B=0.34$ , **c**  $H/B=0.5$

of settlement was observed in  $S/D=4$ . Piles spacing has an effect on two factors: 1—interactions between the piles and 2—volume of enclosed soil between the piles. In  $S/D=2$ , the smallest distance between the piles is observed, in which case the piles cause interactions with each other due to their proximity and reduce the efficiency of the piles. Low piles spacing causes individual piles resistance to not fully mobilize. In addition, the interaction effects of the piles on each other cause more displacement of the piles under the loads. In this case, less volume of soil is enclosed between the piles. The enclosed soil between the piles increases the shear strength. In this case, we have the most interaction effects and the least amount of sand confinement.

In  $S/D=4$ , the interaction effects are insignificant compared to the previous ones due to more piles spacing. In this case, the volume of enclosed soil is higher, and the greatest bearing pressure is observed. In  $S/D=6$ , the lowest pile interaction effects and the maximum amount of enclosed sand are observed. Although large volumes of sand are enclosed in the piles, the effects of enclosed sand on the shear strength decrease due to the large distance between the piles. While in low settlements, piles spacing has a little effect on the load pressure, this effect is remarkable at high settlements. In low settlements, less stress is applied on the soil layer under cushion so the effect of the piles spacing is negligible.

The share of the piles from the total load at different piles spacing was shown in Fig. 12. The highest and lowest portion of piles from the total load is observed in  $S/D=4$  and  $S/D=6$ , respectively. Reduction of interactional effects of piles on each other has led to increase in the force applied to the piles in the  $S/D=4$ . In  $S/D=6$ , the corner and lateral piles undergo less load due to the spacing from the center, which results in reducing the share of the piles in this case.

Figures 13 and 14 show the changes in axial and frictional stress distribution along central (P1) and corner (P3) piles at different piles spacing. Due to the high volume of data, only results related to  $H/B=0.34$  in a medium load (311 kPa) are present here.

The increase of  $S/D$  from 2 to 4 results in reducing the amount of friction in the upper part of the central and corner piles. At  $S/D=2$ , due to the small distance between the piles, pile–soil interactional effects are greater than  $S/D=4$  where this process has increased soil deformation compared to piles and it has increased negative friction further and led to neutral axis transition downwardly. As it is seen in corner piles, more negative friction has been created than central piles.

The maximum and minimum negative friction occurs in  $S/D=6$  and  $S/D=4$ , respectively. Negative friction reduces the force applied to the piles so, as it is seen in previous



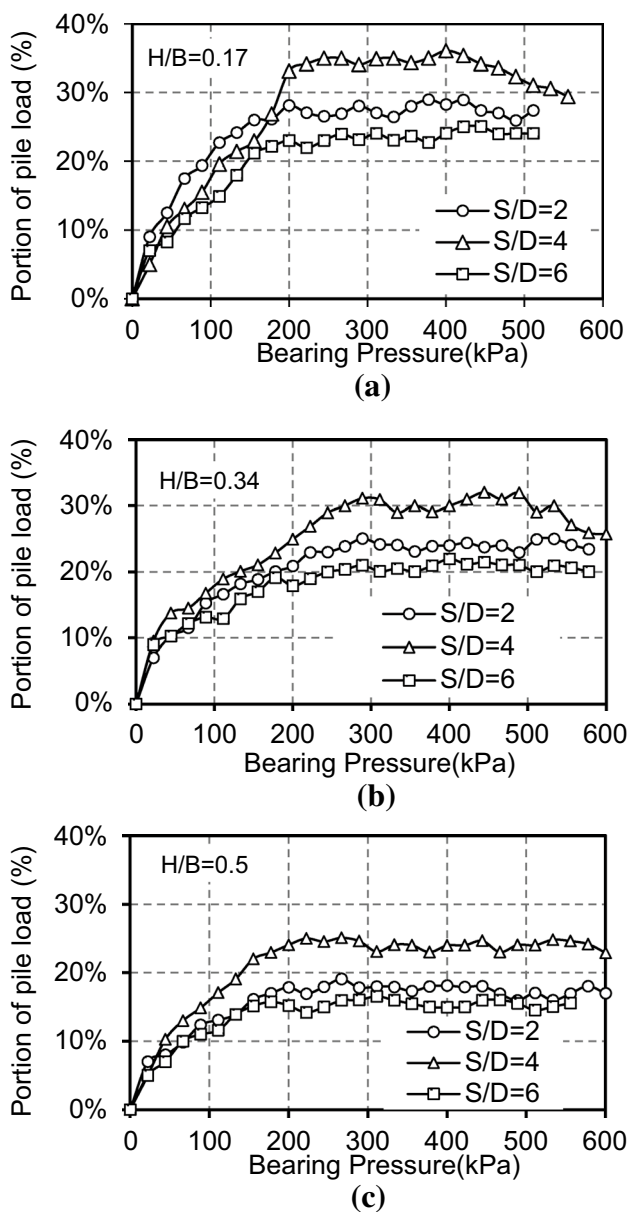


Fig. 12 Variations in the percentage of the share of piles from the total load for different piles spacing a  $H/B=0.17$ , b  $H/B=0.34$ , c  $H/B=0.5$

section, the minimum and maximum portion of piles are observed in  $S/D=6$  and  $S/D=4$  respectively.

Regarding the results of the unreinforced case, the optimum value is in  $H/B=0.34$  and at higher  $H/B$ s, the change of the bearing pressure is negligible. In addition, at different piles spacing, the greatest bearing pressure was observed in  $S/D=4$ . Therefore, in the reinforced tests,  $H/B=0.34$  and  $S/D=4$  were considered.

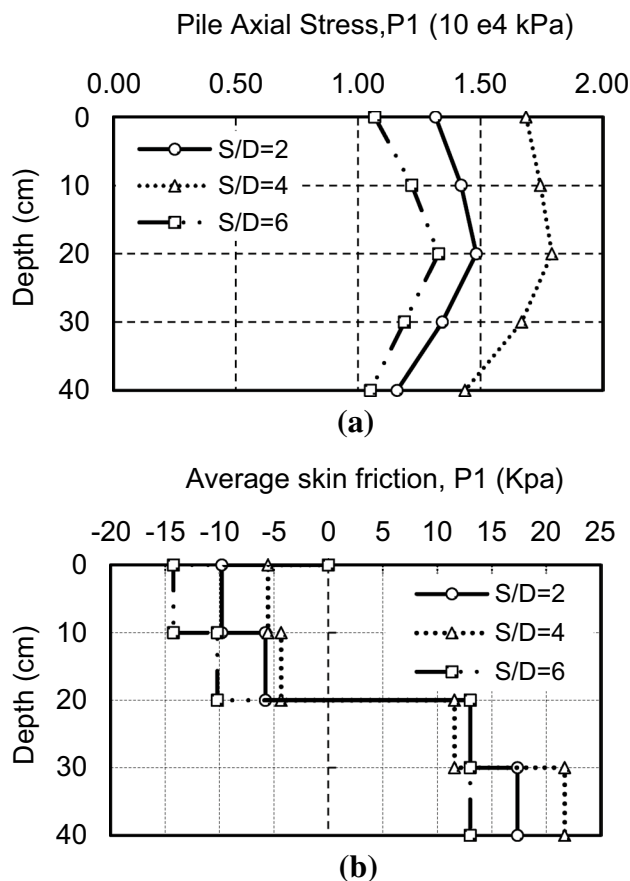


Fig. 13 Variations of axial stress and frictional stress along the central pile (P1) in different piles spacing ( $H/B=0.34$  and  $\sigma=311$  kpa). a Distribution of the axial stress along the pile. b Distribution of the frictional stress along the pile

## 6.2 Reinforced Case

### 6.2.1 Optimum Position of First Layer of Geogrid

With respect to the given results in Sect. 6.1, optimum values observed in the unreinforced case are  $S/D=4$  and  $H/B=0.34$ . Therefore, the studies related to the reinforced case focused on these cases. For this purpose, a geogrid layer with length  $L=6B$  has been placed in different positions of the cushion ( $U/H=0, 0.3, 0.6, 0.9$ ). Figure 15 shows the normalized settlement versus bearing pressure in different positions of the geogrid layer in the cushion. The existence of the geogrid layer increases the bearing pressure. Also in reinforced case, the bearing pressure settlement behavior is stiffer than the unreinforced case. The stiffness is indicated by the inverse slope of bearing pressure settlement in the linear portion of curves.

Figure 16 shows the bearing pressure at various positions of the first layer of the geogrid in the cushion at normalized settlement 2%, 5% and 10%. In low settlements, the bearing

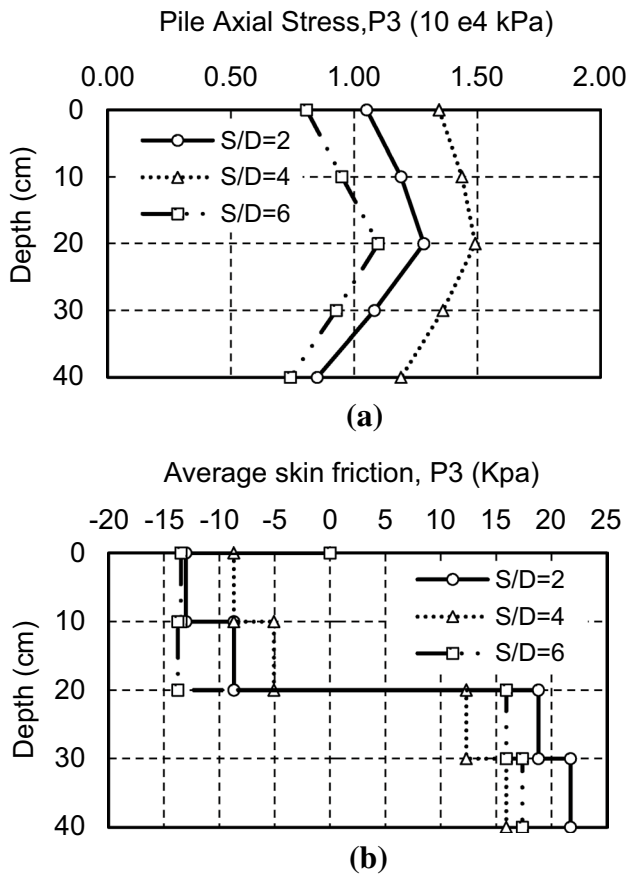


Fig. 14 Variations of axial stress and frictional stress along the corner pile (P3) in different piles spacing ( $H/B=0.34$  and  $\sigma=311$ kpa). **a** Distribution of the axial stress along the pile. **b** Distribution of the frictional stress along the pile

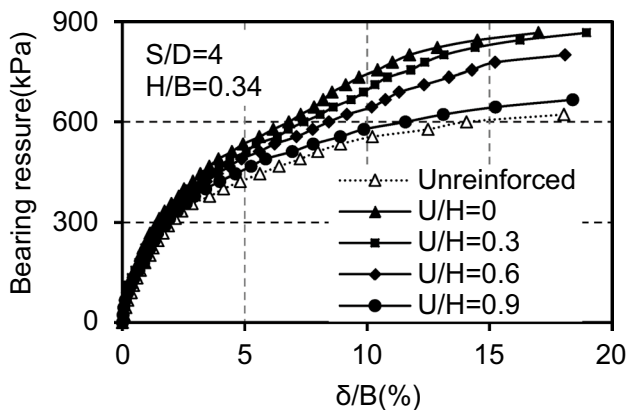


Fig. 15 Variation of bearing pressure versus normalized settlement for different locations of first layer of geogrid

pressures in the tests with and without geogrid are close. In low settlements, deformation of the geogrid is not enough to promote load transfer by membrane effect but with the increase of settlement, the membrane effect of the geogrid

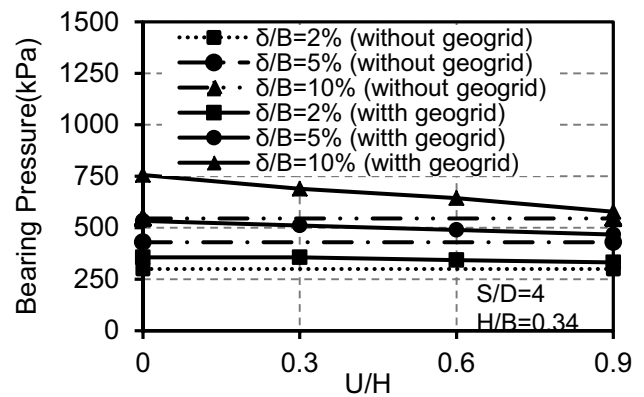


Fig. 16 Variation of bearing pressure versus  $U/H$  in normalized settlements (2%, 5% and 10%)

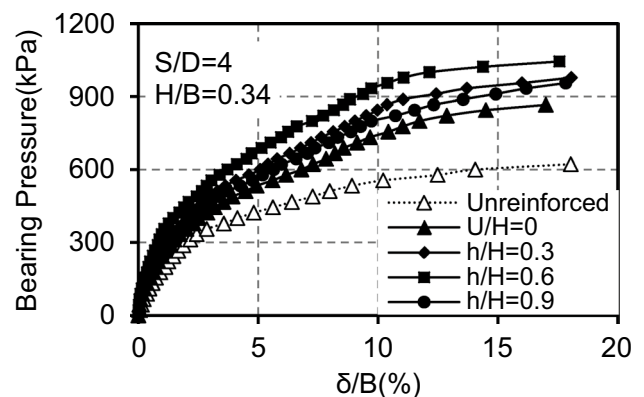


Fig. 17 Variation of bearing pressure versus normalized settlement for different locations of the second layer of the geogrid

is formed and increases the bearing pressure. Increase in the distance of geogrid from the top of piles led to a decrease in the bearing pressure. In the case of  $U/H=0$ , due to the direct transmission of the load to the piles, the force applied to the piles increases and consequently the bearing pressure is also increased. In  $U/H=0.9$  the reinforced and unreinforced behavior are close together. The transition of the geogrid layer upwardly (rise of  $U/H$ ) changes the behavior of the soil from reinforced to unreinforced cases.

### 6.2.2 Optimum Position of Second Layer of Geogrid

To obtain the optimal position for the second layer of geogrid, the first layer of geogrid is placed at optimal position ( $U/H=0$ ). Figure 17 shows bearing pressure at various positions of the second layer of geogrid. It can be seen that the second layer of geogrid plays an important role in the increase of bearing pressure. The existence of the second layer of the geogrid in the cushion causes the vertical loads

to be distributed in the horizontal level and thereby reduces the load transfer to the first layer of the geogrid and increases the bearing pressure. The maximum and minimum bearing pressures were observed at  $h/H=0.6$  and  $h/H=0.9$ , respectively. In  $h/H=0.9$ , the effect of the second layer of geogrid is negligible.

Figure 18 shows the bearing pressure at various positions of the second layer of geogrid ( $h/H=0.3, 0.6, 0.9$ ) in cushion at the normalized settlement of 2%, 5% and 10%. Following the increase of  $h/H$  from 0.3 to 0.6, the bearing pressure is increased and by increase of  $h/H$  from 0.6 to 0.9, the bearing pressure is decreased. Therefore, the minimum settlement and maximum bearing pressure occur in the position of the second layer at  $h/H=0.6$ .

### 6.2.3 Optimum Length for Geogrid Layers

To determine the optimum length for geogrid layers, different lengths of geogrid layers ( $L/B=6, 5, 4, 3, 2, 1$ ) are examined in optimum states ( $H/B=0.34, S/D=4, U/H=0, h/H=0.6$ ). Figure 19 shows bearing pressure versus normalized settlement for different lengths of geogrid. It can be seen that the bearing pressure has been reduced by reducing the length of geogrid layers. Insignificant changes have been observed in reduction of bearing pressure following the decrease of  $L/B$  from 6 to 5 and then to 4 while bearing pressure is extremely decreased by further reduction in  $L/B$  to 3.

By reducing the length of the geogrid, the shear stresses mobilized on the surface between the geogrid and the cushion are reduced as well as the load transfer in the horizontal level. However, in the case of  $L=B$ , the bearing pressure is increased compared with the unreinforced condition. This is because of the direct transfer of the load by geogrid layer to the piles and the enclosure of the soil between the first layer and the second layer that increases the shear strength of the cushion.

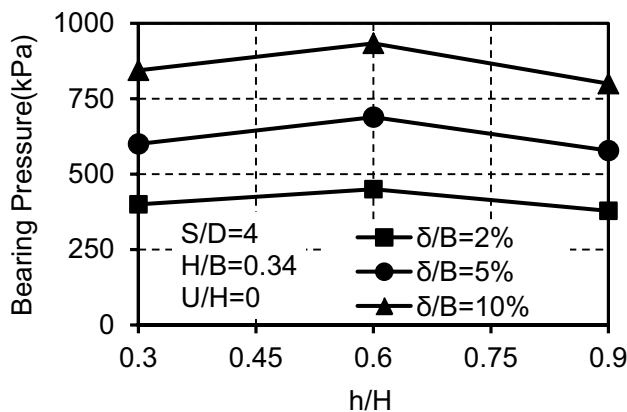


Fig. 18 Variation of bearing pressure versus  $h/H$  for different normalized settlements (2%, 5% and 10%)

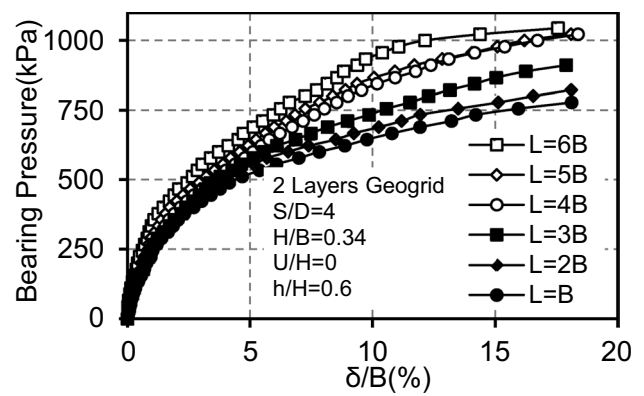


Fig. 19 Variation of the bearing pressure versus normalized settlement for different lengths of the geogrid layers

Figure 20 shows the bearing pressure in different lengths of the geogrid layers in normalized settlements of 2%, 5% and 10%. As can be seen, in low settlements, the length of the geogrid has little effect on bearing pressure. This effect is more significant at higher settlements. The bearing pressure is increased with a high slope as the length of the geogrid is increased from  $L=B$  to  $4B$  while with increase in the length of the geogrid layers from  $L=4B$  to  $6B$ , small variations are seen in the rate of increase of the loading pressure. Thus, the optimum length of the geogrid layer is  $L=4B$ .

### 6.2.4 Portion of Piles from Total Load

Figure 21 shows the share of piles from the total load in reinforced and unreinforced cases at  $S/D=4$  and  $H/B=0.34$ . At the beginning of loading, the portion of piles from the total load is negligible and with increase in the load level, the portion of piles starts to increase rapidly and finally tends to be a constant value. The portion of the piles begins to decrease at the end of loading.

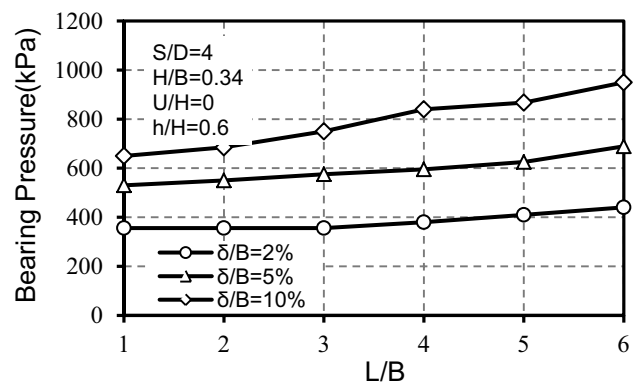
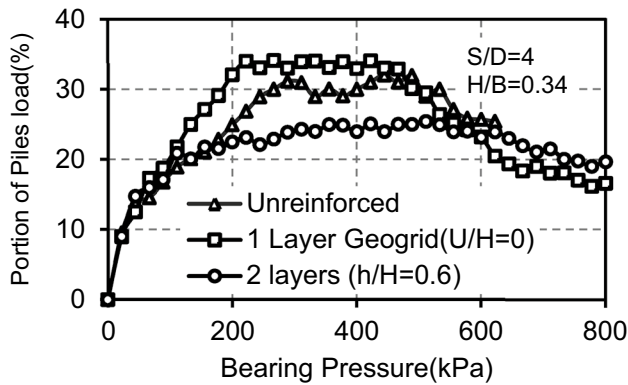


Fig. 20 Variation of bearing pressure versus  $L/B$  in normalized settlements (2%, 5% and 10%)



**Fig. 21** Portion of piles from total load in reinforced and unreinforced cases

There is an insignificant difference between reinforced and unreinforced cases at the low loading levels (< 100 kPa). Following further increase (about 200–500 kPa) in unreinforced case, the portion of piles from the total load is approximately 30%. In the reinforced case with one layer (at  $U/H=0$ ) and two layers ( $U/H=0$  and  $h/H=0.6$ ) of the geogrid, the portion of piles is approximately equal to 34% and 25%, respectively. In high levels of load (> 500 kPa) in both reinforced and unreinforced cases, the portion of piles begins to decrease.

In the presence of a geogrid layer, the excess load created by the vertical component of the tensile force in the geogrid increases the portion of the piles from the total load. Although in this case, a portion of the vertical load is transferred by the geogrid layer to the horizontal plane in the cushion, but this load transfer occurs at high settlements. Before the excessive settlements occur and the membrane effect of the geogrid starts, the additional force is tolerated by the piles. In the presence of two layers of geogrid, the upper layer of the geogrid depletes part of the load and less load is tolerated by the lower geogrid layer. This phenomenon causes less load to be transferred by the piles and has been mentioned by Deb et al. [23].

### 6.2.5 Distribution of Axial and Skin Frictional Stress in Piles

Figures 22 and 23 show the axial and frictional stress distribution along the central pile (P1) and corner piles (P3) in unreinforced, reinforced with one layer and two layers of the geogrid in an average stress of 311 kPa. 311 kPa was chosen because at this load level, the portion of the piles from the total load is almost constant and at this level, the foundations in both reinforced and unreinforced conditions have not reached their final bearing capacity.

The axial force in the piles changes linearly with increasing load. In all cases, in the upper part of the corner piles, the negative friction is formed due to the greater

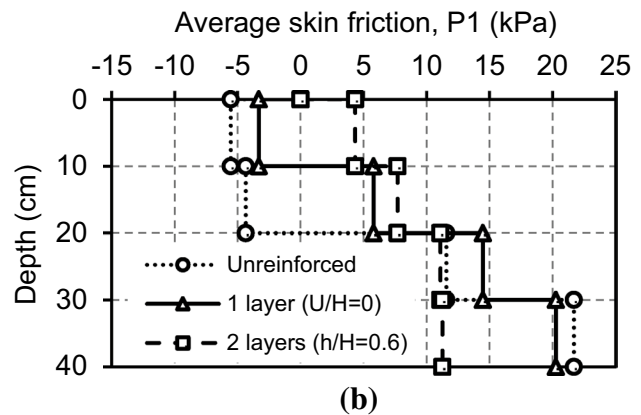
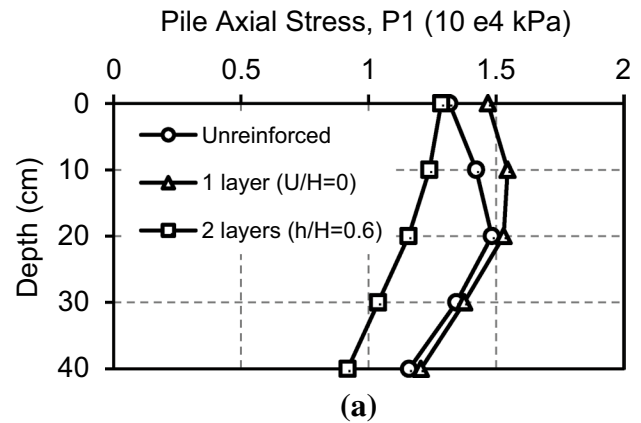


**Fig. 22** Variations of axial stress and frictional stress along the central pile (P1) in reinforced and unreinforced cases. **a** Distribution of the axial stress along the pile. **b** Distribution of the frictional stress along the pile

displacement of the soil relative to the pile. The amount of negative friction in the unreinforced condition is greater than that of the reinforced case, which reduces the force applied to the pile compared with the reinforced case. In the central pile in case of unreinforced and reinforced with a geogrid layer, a negative friction in the upper part of the pile was created, but in the case of two layers of the geogrid, no negative friction was created.

As shown in Fig. 22b and 23b, the addition of geogrid layers to the cushion reduces negative friction in the upper parts of the piles and thus reduces the difference between the positive and negative frictional forces along the piles. Therefore, it can be concluded that the use of geogrid layers causes a more uniform distribution of forces in the piles.

The cushion layer confined between the two-layer geogrids acts similar to an assumed raft at the top of piles and applies this behavior to connected pile raft and therefore negative friction is not created. Negative friction is further created in corner piles than in the central pile.

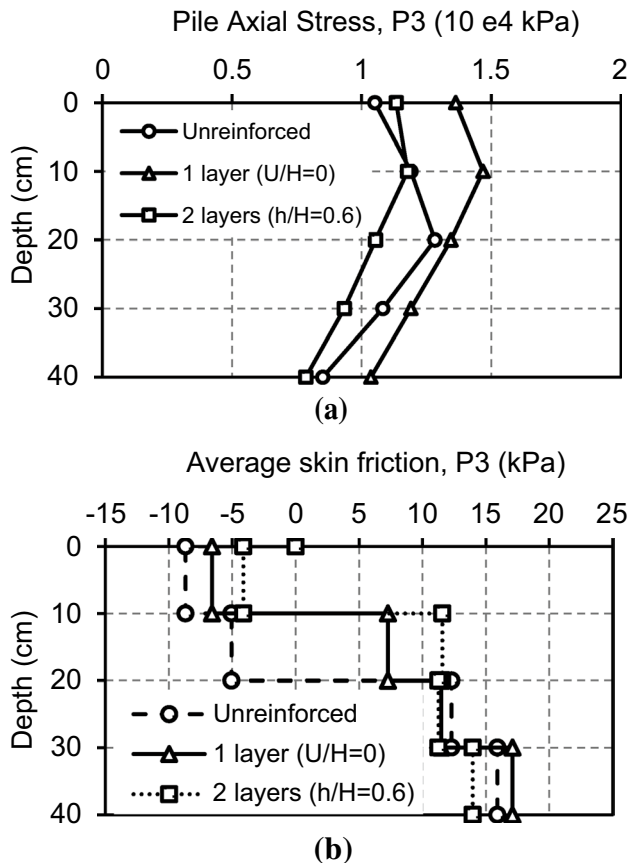


**Fig. 23** Variations of axial stress and frictional stress along the corner pile (P3) in reinforced and unreinforced cases. **a** Distribution of the axial stress along the pile. **b** Distribution of the frictional stress along the pile

## 7 Conclusion

Based on the conducted tests on the non-connected pile raft in both reinforced and unreinforced cases, the following results were obtained:

1. In unreinforced case, the highest bearing pressure has been observed in a certain thickness of the cushion. With a further increase in the thickness of the cushion, a slight increase has been observed in the bearing pressure. The optimum thickness of the cushion was observed at  $H/B=0.34$ .
2. In unreinforced case, the amount of force applied to the piles decreases with increase in the thickness of the cushion. In addition, in the upper part of the piles, a negative friction is created and the neutral axis moved to the top of the pile by increasing the thickness of the cushion.
3. In the unreinforced case, at a given pile spacing, the greatest bearing pressure has been observed. As  $S/D$  increases from 2 to 4 and from 4 to 6, the bearing pres-

sure increases and decreases, respectively. Also in  $S/D=4$ , the maximum force applied to the piles and the lowest negative friction in the upper part of the piles were observed.

4. In all cases (reinforced and unreinforced), in the corner piles, there is further negative friction compared with the central pile that causes the neutral axis to move downwards in the corner piles.
5. In the presence of a geogrid layer, the maximum bearing pressure occurs when the geogrid is located on the bottom of the cushion ( $U/H=0$ ). In this case, the portion of the piles from the total load increases, less negative friction in the pile was created compared to the unreinforced case, and the neutral axis moves upwards to the top of the pile.
6. The optimum position of the second layer of the geogrid is at  $h/H=0.6$ . In this case, there is less negative friction in the upper part of the pile compared with conditions of the unreinforced and reinforced with a geogrid layer.
7. The optimum length of the geogrid layers was  $4B$ . Further increase of the length of the layers of the geogrid has little effect on increase in the bearing pressure.

**Funding** Self-funded—not applicable.

## References

1. Baziar MH, Kashkooli A, Saedi-Azizkandi A (2012) Prediction of pile shaft resistance using cone penetration tests (CPTs). *Comput Geotech* 45:74–82
2. Baziar MH, Azizkandi AS, Kashkooli A (2015) Prediction of pile settlement based on cone penetration test results: an ANN approach. *KSCE J Civ Eng* 19(1):98–106
3. Azizkandi AS, Kashkooli A, Baziar MH (2014) Prediction of uplift pile displacement based on cone penetration tests (CPT). *Geotech Geol Eng* 32(4):1043–1052
4. Blanc M, Rault G, Thorel L, Almeida M (2013) Centrifuge investigation of load transfer mechanisms in a granular mattress above a rigid inclusions network. *Geotext Geomembr* 36:92–105
5. Moayed RZ, Izadi E, Mirsepahi M (2013) 3D finite elements analysis of vertically loaded composite piled raft. *J Cent South Univ* 20(6):1713–1723
6. Di Prisco C, Pisanò F (2014) Numerical modeling and mechanical analysis of an innovative soil anchoring system. *Acta Geotech* 9(6):1013–1028
7. Tradigo F, Pisanò F, Prisco CD, Mussi A (2015) Non-linear soil-structure interaction in disconnected piled raft foundations. *Comput Geotech* 63:121–134
8. Liang FY, Chen LZ, Shi XG (2003) Numerical analysis of composite piled raft with cushion subjected to vertical load. *Comput Geotech* 30:443–453
9. Fu Q, Liu H, Ding X, Zheng C (2015) Numerical investigation of piled raft foundation in mitigating embankment vibrations induced by high-speed trains. *J Cent South Univ* 22(11):4434–4444
10. Huang M, Liang FY, Li Z (2007) Recent advances of pile foundation in China. In: *Proceedings of the International Workshop on Recent Advances of Deep Foundations*, Yokosuka, Japan, pp 1–2

11. Eslami A, Salehi Malekshah S (2011) Analysis of non-connected piled raft foundations (NCPRF) with cushion by finite element method. *Comput Methods Civ Eng* 2(2):153–168
12. Han XL, Xiao CA, Li JX et al (2013) Spring constitutive model of rigid pile composite foundation and application in design of raft foundation. *J Cent South Univ* 20(4):1079–1084
13. Wong LH, Chang MF, Cao XD (2000) Raft foundations with disconnected settlement reducing piles. Design application of raft foundations and ground slabs, Chap. 17, Thomas Telford, London, pp 469–486
14. Tradigo F, Pisanò F, Mussi A, Persio R, di Prisco CG (2014) Finite element analysis of soil–structure interaction in disconnected piled raft foundations. In: Hicks MA, Brinkgreve, Ronald BJ, Rohe A (eds) Numerical methods in geotechnical engineering (NUMGE). II. CRC Press (Taylor & Francis Group), Delft, Netherlands, pp 705–710
15. Haghbin M (2014) Study on behavior of soil reinforcing pile in piled raft systems. *Int J Civil Eng* 12(4):304–315
16. Shahu JT, Madhav MR, Hayashi S (2000) Analysis of soft ground—granular pile–granular mat system. *J Comput Geotech* 27(1):45–62
17. Zhang H, Shi ML (2012) Mechanical performance of settlement-reducing pile foundation with cushion. *Adv Mat Res* 368–373:2545–2549
18. Cao XD, Wong IH, Chang MF (2004) Behaviour of model rafts resting on pile-reinforced sand. *J Geotech Geoenviron Eng* 130(2):129–138
19. El Sawwaf M (2010) Experimental study of eccentrically loaded raft with connected and unconnected short piles. *J Geotech Geoenviron Eng* 136(10):1394–1402
20. Sawada K, Takemura J (2014) Centrifuge model tests on piled raft foundation in sand subjected to lateral and moment loads. *Soils Found* 54(2):126–140
21. Saeedi Azizkandi A, Baziar M, Rasouli H, Modarresi M, Shahnazari H (2015) Centrifuge modeling of non-connected piled raft system. *Int J Civ Eng* 13(2):114–123
22. Xing HF, Zhang Z, Liu HB et al (2014) Large-scale tests of pile-supported earth platform with and without geogrid. *Geotext Geomembr* 42:586–598
23. Deb K, Basudhar PK (2007) Generalised model for geosynthetic-reinforced granular fill-soft soil with stone column. *Int J Geomech ASCE* 7(4):266–276
24. Han J, Gabr MA (2002) Numerical analysis of geosynthetic-reinforced and pile-supported earth platform over soft soil. *J Geotech Environ Eng ASCE* 128(1):44–53
25. Abusharar SW, Zheng J-J, Chen B-G, Yin J-H (2009) A simplified method for analysis of a piled embankment reinforced with geosynthetics. *Geotext Geomembr* 27(1):39–52
26. Chen R, Xu Z, Chen Y, Ling D, Zhu B (2010) Field tests on pile-supported embankments over soft ground. *J Geotech Geoenviron Eng ASCE* 136(6):777–785
27. Naughton PJ, Kempton GT (2005) Comparison of analytical and numerical analysis design methods for piled embankments. Contemporary issues in foundation engineering. In: Rathje EM (ed) Proc. Geo-Frontiers 2005, Austin, Geotechnical Special Publication (GSP) 131. ASCE, Reston, VA, USA
28. Fioravante V, Giretti D (2010) Contact versus noncontact piled raft foundations. *Can Geotech J* 47(11):1271–1287
29. Saeedi Azizkandi A, Baziar MH, Modarresi M, Salehzadeh H, Rasouli H (2014) Centrifuge modeling of pile-soil-pile interaction considering relative density and toe condition. *Sci Iran* 21(4):1330–1339
30. Baziar MH, Rafiee F, Lee CJ, Saeedi Azizkandi A (2018) Effect of superstructure on the dynamic response of nonconnected piled raft foundation using centrifuge modeling. *Int J Geomech ASCE* 18(10):04018126–04018121
31. Azizkandi AS, Baziar MH, Yeznabad AF (2018) 3D dynamic finite element analyses and 1g shaking table tests on seismic performance of connected and nonconnected piled raft foundations. *KSCE J Civ Eng* 22(5):1750–1762
32. Bolton MD, Gui MW, Garnier J, Corte JF, Bagge G, Laue J, Renzi R (1999) Centrifuge cone penetration tests in sand. *Geotechnique* 49(4):543–552
33. Gui MW, Bolton MD, Garnier J, Corte JF, Bagge G, Laue J, Renzi R (1998) Guidelines for cone penetration tests in sand. In Proceedings of international conference centrifuge, vol. 98. Rotterdam, Netherlands, pp 155–160
34. Gui MW, Bolton MD (1998) Geometry and scale effects in CPT and pile design. In: Proceedings of the 1st International Conference on Geotechnical Site Characterization. Atlanta, GA, USA, pp. 1063–1068
35. Jenck O, Dias D, Kastner R (2005) Soft ground improvement by vertical rigid piles two-dimensional physical modelling and comparison with current design methods. *Soils Found* 45(6):15–30
36. British Standard BS8006 (1995) Code of practice for strengthened/reinforced soils and other fills. British Standard Institution, London